Journal of Solid State Chemistry 184 (2011) 770–777

Contents lists available at ScienceDirect

Journal of Solid State Chemistry

journal homepage: www.elsevier.com/locate/jssc

Insertion-release of guest species and ionic conduction in polyoxometalate solids with a layer-like Anderson structure

Haruo Naruke [a,*], Naoyuki Kajitani [a], Takayuki Konya [b]

[a] Chemical Resources Laboratory, Tokyo Institute of Technology, R1-23, 4259 Nagatsuta, Midori-ku, Yokohama 226-8503, Japan
[b] Rigaku Corporation, 3-9-12, Matsubara-cho, Akishima-shi, Tokyo 196-8666, Japan

ARTICLE INFO

Article history:
Received 29 September 2010
Received in revised form
20 January 2011
Accepted 23 January 2011
Available online 1 February 2011

Keywords:
Polyoxometalate
Anderson-type
Crystal structure
Ionic conduction

ABSTRACT

The precipitation of Na^+ and K^+ mixed salts of Anderson type $[SbW_6O_{24}]^{7-}$ by addition of excess of $NaNO_3$ and NaCl yielded polycrystalline powders of $Na_{2.5}K_{5.3}[SbW_6O_{24}](NO_3)_{0.8}\cdot 12H_2O$ (**1**) and $Na_2K_{5.35}[SbW_6O_{24}]Cl_{0.35}\cdot 12H_2O$ (**2**), respectively. The two compounds are isomorphous and exhibit a layer-like Anderson (LLA) type structure, which consists of $[SbW_6O_{24}]^{7-}$-containing layers and interstitial Na^+, K^+, NO_3^- or Cl^-, and water O atoms. Recrystallization of **1** and **2** from hot water yielded $Na_2K_{5.4}[SbW_6O_{24}](NO_3)_{0.4}\cdot 12H_2O$ (**1-recry**) and $Na_2K_{5.25}[SbW_6O_{24}]Cl_{0.25}\cdot 12H_2O$ (**2-recry**) as a result of partial release of NO_3^- and Cl^- (and Na^+ and K^+ for charge compensation). Dehydration of **1** and **2** at 400 and 500 °C (**1-dehyd400** and **2-dehyd500**) caused a shrinkage of lattice, but their the LLA structures retained. Simulation of X-ray diffraction (XRD) patterns for the dehydrated forms allowed to presume that the each $[SbW_6O_{24}]^{7-}$ anion had been 30°-rotated within its molecular plane in order to avoid intermolecular repulsion. A compressed powder of **1-dehyd400** exhibited fast alkaline-ion conduction with a bulk conductivity of $1.2\times10^{-2}\,\Omega^{-1}\,cm^{-1}$ at 400 °C. The hosting of a sufficient amount of NO_3^- together with Na^+ for charge compensation into the lattice is crucial for high conduction.

1. Introduction

A hexanuclear metal oxide cluster referred to as "Anderson structure" [1–4] with a general formula $[XM_6O_{24}]^{p-}$ (*X*: heteroatom; *M*=Mo and W) is one of the well-defined family of polyoxometalates (POMs) [5,6]. The Anderson structure exhibits a characteristic planar configuration with an idealized point symmetry of $\bar{3}m$ (D_{3d}), and consists of a central $\{XO_6\}$ octahedron edge-shared by surrounding six $\{MO_6\}$ octahedra in a hexagonal arrangement (Scheme 1 left). The heteroatom *X* includes metallic and non-metallic elements in wide oxidation states from +2 to +7 [5,6]. As is often drawn [3], POMs can be regarded as nano-sized molecular fragments of general non-molecular metal oxides in view point of both structures and physicochemical properties. In fact, a $\{M_7O_{24}\}$ framework unit with the Anderson structure is observable in numerous CdI_2 (or brucite) type layered metal oxides possessing a $\{MO_2\}$-sheet structure (Scheme 1 right). Examples of such oxides include $M(OH)_2$ (*M*=Ca, Mg, Cd, Mn, Co, Ni) [7] and alkaline metal intercalated derivatives AMO_2 (*A*=alkaline metals) [8,9]. The same $\{MO_2\}$-sheet is found in layered double hydroxides (LDHs) [10] with a typical formula $[M'^{II}_xM''^{III}_{1-x}(OH)_2](CO_3)_{x/2}\cdot nH_2O$ ($M'^{II}=Mg^{2+}$, Zn^{2+}; $M''^{III}=Al^{3+}$, Ga^{3+}). Beside the metal oxides, metal dihalogenides MHa_2 (*Ha*=F, Cl, Br, I) and dichalcogenides MCh_2 (*Ch*=S, Se, Te) belong to this structural type [7,11]. Some of these compounds are candidate cathode materials for rechargeable batteries due to their capability of intercalation–deintercalation of guest ions involving redox reactions [12].

In a majority of Anderson type POMs, the anions are arranged in parallel in the lattices, i.e., anions' $\bar{3}$ axes point to same orientation. Of such structures, however, there are only a few examples in which the anions are packed in coplanar (Scheme 2 left). In this packing mode, an anion and its neighboring anions are aligned in a plane to form a $\{XM_6O_{24}\}$-sheet, and counter cations and waters of crystallization are positioned between the sheets (Scheme 2 left). This structural feature, so-called layer-like Anderson (LLA) type here, bears a close similarity to the crystal structures of above-mentioned layered compounds (Scheme 2 right). One may expect that, in analogy to the layered compounds, the LLA type POMs also have ability for hosting and releasing of guest molecules, and cation transport in the lattices.

We describe here the fact that $Na_2K_5[SbW_6O_{24}]\cdot 12H_2O$ with the LLA structure type first reported by Lee et al. [13] crystallizes incorporating NO_3^- and Cl^- anions (and charge compensating cations) in its interlayer space to yield $Na_{2.5}K_{5.3}[SbW_6O_{24}](NO_3)_{0.8}\cdot 12H_2O$ (**1**) and $NaK_6[SbW_6O_{24}](NaCl)_{0.35}\cdot 14H_2O$ (**2**),

* Corresponding author. Fax: +81 45 924 5271.
E-mail address: hnaruke@res.titech.ac.jp (H. Naruke).

0022-4596/$ - see front matter © 2011 Elsevier Inc. All rights reserved.
doi:10.1016/j.jssc.2011.01.033

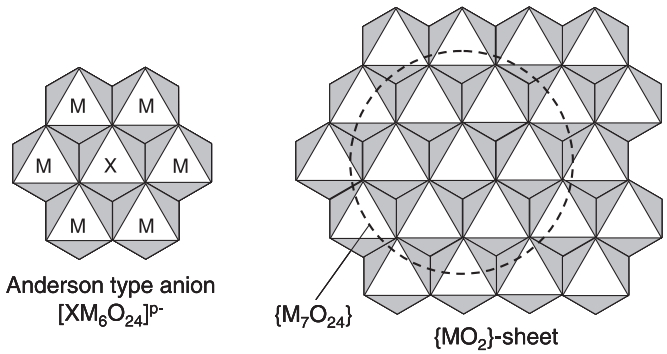

Scheme 1. Anderson type POM (left) and $\{MO_2\}$-sheet in $M(OH)_2$ (right).

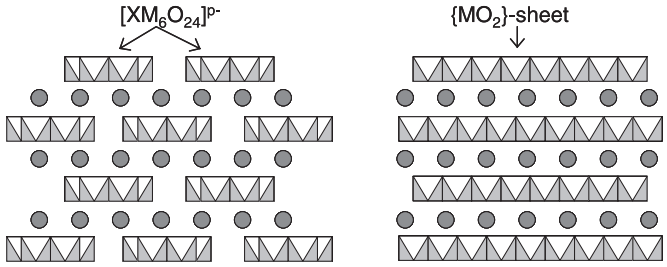

Scheme 2. Layer-like Anderson (LLA) type POM (left) and $\{MO_2\}$-based layer compound. The gray circles are interstitial ions and/or molecules.

respectively. The compounds **1** and **2** release a part of their guest anions in the recrystallization procedures. They also show reversible deintercalation–intercalation of waters of crystallization involving lattice contraction and recovery retaining the LLA structure. Furthermore, we discovered that the dehydrated polycrystalline samples have relatively high cationic (Na^+ and K^+) conductivity ($1.2\times10^{-2}\,\Omega^{-1}\,cm^{-1}$ at 400 °C for **1**). It is well known that some of Keggin type POM crystals in acid forms (H^+ salts) are excellent proton conductors at room temperature [14,15]. However, their practical application is limited by spontaneous dehydration that resulted in a significant drop of conductivity [15]. Recently, ionic conduction of a polyoxomolybdate was reported [16], but the conductivity declined above room temperature because of dehydration. The present study describes the first POM-based alkali ion conductor that operates upon dehydrated conditions.

2. Experimental

2.1. Syntheses of $Na_{2.5}K_{5.3}[SbW_6O_{24}](NO_3)_{0.8}\cdot 12H_2O$ (1) and $Na_2K_{5.4}[SbW_6O_{24}](NO_3)_{0.4}\cdot 12H_2O$ (1-recry)

Tungsten trioxide (WO_3: 5.2 g, 22.4 mmol) was dissolved to a hot (80 °C) potassium hydroxide solution (KOH: 3.0 g, 53 mmol; H_2O: 40 ml). A paste of $K[Sb(OH)_6]$ (1.0 g, 3.8 mmol) which had been ground with a small portion of water in an agate mortar was added to the tungstate solution, heated with stirring to complete dissolution, and cooled to ca. 40 °C. The solution was acidified to pH 7.2 with concentrated nitric acid (HNO_3: 13 M), and a few residuals were filtered off. Immediately, an aqueous solution (15 ml) of sodium nitrate ($NaNO_3$: 6.8 g, 80 mmol) was added to the filtrate with vigorous stirring to yield white precipitates, and continued stirring for 30 min. A microcrystalline solid of **1** (yield: 5.0 g; 63% based on W) was collected by vacuum filtration and dried overnight in an ambient atmosphere. Found: H: 1.13; N: 0.52; Na: 2.79; K: 9.64; Sb: 5.82; W: 50.8 wt%. Calcd for $Na_{2.5}K_{5.3}[SbW_6O_{24}](NO_3)_{0.8}\cdot 12H_2O$: H: 1.13; N: 0.52; Na: 2.69; K: 9.69; Sb: 5.69; W: 51.56 wt%. Single crystals (**1-recry**) suitable for X-ray crystallography were grown by recrystallization of whole amount of **1** from hot water (70 °C, 80 ml). The recrystallization caused a partial release of NO_3^- and charge compensating Na^+ and K^+ cations. Found: H: 1.14; N: 0.26 Na: 2.12; K: 9.99; Sb: 5.88; W: 51.4 wt%. Calcd. for $Na_2K_{5.4}[SbW_6O_{24}](NO_3)_{0.4}\cdot 12H_2O$: H: 1.15; N: 0.27; Na: 2.18; K: 10.02; Sb: 5.78; W: 52.35 wt%.

2.2. Syntheses of $Na_2K_{5.35}[SbW_6O_{24}]Cl_{0.35}\cdot 12H_2O$ (2) and $Na_2K_{5.25}[SbW_6O_{24}]Cl_{0.25}\cdot 12H_2O$ (2-recry)

Microcrystalline powders (**2**) and single crystals (**2-recry**) were obtained in similar preparation procedure as **1** using hydrochloric acid (HCl, 12 M) and sodium chloride (NaCl: 4.7 g, 80 mmol) for acidification and precipitation reagents, respectively. The yield was 2.8 g (36% based on W). Found: H: 1.30; Na: 2.33; Cl: 0.58; K: 9.90; Sb: 5.95; W: 51.5 wt%. Calcd for $Na_2K_{5.35}[SbW_6O_{24}]Cl_{0.35}\cdot 12H_2O$: H: 1.16; Na: 2.20; Cl: 0.59; K: 10.00; Sb: 5.82; W: 52.7 wt%. Single crystals (**2-recry**) suitable for X-ray crystallography were grown by dissolution and recrystallization from minimum volume of hot water (70 °C). Found: H: 0.97; Na: 2.30; Cl: 0.42 K: 9.84; Sb: 5.96; W: 52.5 wt%. Calcd for $Na_2K_{5.25}[SbW_6O_{24}]Cl_{0.25}\cdot 12H_2O$: H: 1.16; Na: 2.21; Cl: 0.43; K: 9.84; Sb: 5.84; W: 52.9 wt%.

2.3. X-ray structure determination

Air-stable single crystals of **1-recry** and **2-recry** with an octahedral shape were fixed on glass fibers and mounted on a Rigaku RAXIS-RAPID imaging plate diffractometer with monochromatized Mo$K\alpha$ (0.72069 Å) radiation. Reflection data were collected at 298 K. Initial positions for Sb and W were determined by a direct method using SHELX 97 [17], and other atoms were determined with difference Fourier synthesis. Structural parameters were refined with full-matrix least-squares method using CRYSTALS [18] in a structural analysis software package CrystalStructure [19]. A numerical absorption collections SHAPE [20] and NUMABS [21] were applied. Hydrogen atoms were not included in the calculation. All of the atoms were refined anisotropically. Atomic occupancies for Na^+ and K^+ cations and NO_3^- (for **1-recry**) and Cl^- (for **2-recry**) anions were fixed based on their elemental analysis. Details of measurement conditions, final structural parameters, and convergence factors for **1-recry** and

Table 1
X-ray crystallographic data of **1-recry** and **2-recry**.

	1-recry	2-recry
Formula	$Na_2K_{5.4}[SbW_6O_{24}](NO_3)_{0.4}\cdot 12H_2O$	$Na_2K_{5.25}[SbW_6O_{24}]Cl_{0.25}\cdot 12H_2O$
M.W.	2106.93	2085.13
Crystal system	Trigonal	Trigonal
Space group (No.)	$R\bar{3}m$ (1 6 6)	$R\bar{3}m$ (1 6 6)
a/Å	13.266(7)	13.288(8)
c/Å	18.534(14)	18.548(13)
V/Å^3	2825(3)	2836(3)
Z	3	3
D_c/Mg cm^{-3}	3.716	3.662
μ/mm^{-1}	19.708	19.625
[a] R_1 [$I<2\sigma(I)$]	0.0191	0.0461
[b] wR_2 (all data)	0.0502[c]	0.1334[d]
GOF	0.901	1.035
$\Delta\rho_{min}$, $\Delta\rho_{max}$ /eÅ^{-3}	1.70, −2.08	2.32, −2.19

[a] $R_1=(\Sigma||F_o|-|F_c||)/(\Sigma|F_c|)$.
[b] $wR_2=\Sigma[w(F_o^2-F_c^2)^2]/\Sigma[w(F_o^2)^2]^{1/2}$.
[c] $w=[\{0.0004F_o^2+0.2000\sigma(F_o^2)+0.0004\}/(4F_o^2)]^{-1}$.
[d] $w=[\{0.0027F_o^2+0.6000\sigma(F_o^2)\}/(4F_o^2)]^{-1}$.

Table 2
Selected interatomic distances (Å) in **1-recry**.

Sb–O3	×6	1.933(4)	K–O1	×2	2.851(3)
W–O1	×2	1.750(3)		×2	2.885(3)
W–O2	×2	1.955(2)	K–O3	×1	3.031(5)
W–O3	×2	2.219(4)	K–O5	×2	3.018(4)
N–O4	×3	1.32(2)	K–O6	×1	2.999(7)
Na–O5	×3	2.372(6)		×1	3.517(7)
Na–O6	×3	2.388(9)	K–O4	×1	3.15(2)

2-recry are listed in Table 1. Table 2 lists the selected interatomic distances in **1-recry**. Further details of the crystal structure investigation(s) may be obtained from Fachinformationszentrum Karlsruhe, 76344 Eggenstein-Leopoldshafen, Germany (fax: (+49)7247-808-666; e-mail: crysdata@fiz-karlsruhe.de, http://www.fiz-karlsruhe.de/request_for_deposited_data.html) on quoting the appropriate CSD numbers (**1-recry**: CSD-421675; **2-recry**: CSD-421676).

High temperature (375 °C) in-situ powder X-ray diffraction (XRD) pattern of **1** dehydrated in a nitrogen atmosphere was performed using Rigaku TTR II diffractometer equipped with a Reactor X in the 3–90° range (interval: 0.02°) with a counting time 3 s per datum. The structure was refined using the Rietveld method [22,23] based on the observed pattern. Details on the refinement procedure and results are shown in Section 3and Supporting information.

2.4. Dehydration of samples and ionic conductivity measurement

The microcrystalline powders of **1** and **2** were dehydrated by heating in a furnace at 400–500 °C for 6 h to form bulky powders denoted with **1-dehyd400**, **1-dehyd500**, **2-dehyd400**, and **2-dehyd500**. The dehydration was also carried out for **1-recry** at 400 °C for 6 h to yield **1-recry-dehyd400**. All of the dehydrated samples were immediately compressed into disks with a diameter of 10 mm at a pressure of ca. 2 kNcm^{-2}. The disk was clamped with two mirror-polished Pt disk electrodes (diameter: 10 mm) and placed in a nitrogen or argon gas flow in a temperature-controlled quartz chamber. The ac. impedance of the sample was measured on an HP4192A impedance analyzer at 200–400 °C (200–500 °C for **2-dehyd-500**) with an interval of 20 °C. The measurement was carried out in the frequency range of 5 Hz–10 MHz and at the application potential 1.0 V. Four terminal pair connection was employed for canceling a float impedance. Data were analyzed with software EIS Spectrum Analyzer [24].

2.5. Other measurements

Infrared spectra were obtained with JASCO FTIR 410 using KBr method. Room-temperature XRD patterns were measured on a Rigaku Rint Ultima+/PC diffractometer with monochromatized Cu$K\alpha$ (1.5418 Å) radiation in the range of 5–60° (interval: 0.02°) with a scan rate of 2° min^{-1}. Thermogravimetric (TG) and differential thermal analysis (DTA) were made using ULVAC MTS9000+TGD9600 system. Microscopic mapping of Na, K, Sb, and W on a cross section of electrolyzed disk of **1** (see text for details) were obtained with X-ray probe microanalyzer (EDAX EAGLE μ-Probe). Elementary analyses of C, N, and H were performed on a Yanaco MT 5 CHN CORDER. Sb and W contents were analyzed by inductively coupled plasma atomic emission spectroscopy on an ICPS-8100 spectrometer.

3. Results and discussion

3.1. Description of structures

The compound **1-recry**, isostructural with $Na_2K_5[SbW_6O_{24}]\cdot 12H_2O$,[9] consists of $[SbW_6O_{24}]^{7-}$ anion, Na^+ and K^+ cations, waters of crystallization, and NO_3^- anions. The $[SbW_6O_{24}]^{7-}$ anion has an ideal symmetry of $\bar{3}m$ (D_{3d}) (Fig. 1(a)), where Sb is imposed on 3*a* site (Wyckoff notation). The Sb–O3 distance in the $\{SbO_6\}$ octahedron is 1.993(4) Å, and the terminal W=O1 and bridging W–O2 and W–O3 distances are 1.750(3), 1.955(4), and 2.217(5) Å, respectively. The geometric feature of $[SbW_6O_{24}]^{7-}$ is comparable to that in the same anion in $Na_2K_5[SbW_6O_{24}]\cdot 12H_2O$ [13] and $K_{5.5}H_{1.5}[SbW_6O_{24}]\cdot 6H_2O$ [25]. Fig. 1(b) shows the structure of **1-recry** viewed parallel to the (0 0 1) plane, where the anions are stacked in the [0 0 1] direction with a *d*-spacing of 6.18 Å (=*c*/3). The Na atom, which is positioned near to the $\{SbW_6O_{24}\}$-sheet, is octahedrally coordinated with six water oxygens (of three O5 and three O6 atoms), while the K atom positioned at the interlayer space is multi-bonded with oxygens of water (O5 and O6) and nitrate (O4), and interlinks the $\{SbW_6O_{24}\}$-sheet via O1–K–O3 bonding. The most significant feature of **1-recry** is the NO_3^- group in its interlayer space with an occupancy of 0.4 molecule per $[SbW_6O_{24}]^{7-}$ anion; the presence of this anion is supported by IR absorption bands centered at 1355 and 1385 cm^{-1} (Fig. 4), and the nitrogen analysis (found, 0.26; calculated, 0.26 wt%). The central N atom in NO_3^- is positioned on the 3*b* ($\bar{3}m$) site, and therefore, two symmetry-related NO_3^- molecules are superimposed to form a pseudo $\{NO_6\}$ group, which has an approximate planar configuration parallel to the (0 0 1) plane (Fig. 2). Similar disordering of NO_3^- has been reported for KNO_3 [26–28]. The six K^+ cations surround the $\{NO_6\}$ group with a hexagonal arrangement, and coordinate to the nitrate O4 atoms with a distance of 3.152(5) Å. Similar cationic environment around NO_3^- is achieved in KNO_3 polymorphs [26–28], in which, however, six K^+ cations are located in crown-like zigzag configuration. The N–O distance 1.32(1) Å is longer than those (1.24–1.27 Å) in KNO_3 [26–28]. This may be due to the effective interaction between the nitrate O4 and K in planar-arrangement. The Na^+ cation on the crystallographic $\bar{3}$ axis is located in proximity to the $\{SbW_6O_{24}\}$-sheet. From the elemental analysis and charge balance, we presumed full (100%) and 90% occupancies for the Na and K sites, respectively, throughout the structure refinement. In comparison with the corresponding occupancies of Na (100%) and K (83.3%=5/6) in $Na_2K_5[SbW_6O_{24}]\cdot 12H_2O$ [13], **1-recry** is well described as an inclusion compound comprising $Na_2K_5[SbW_6O_{24}]\cdot 12H_2O$ and 0.4 KNO_3.

Fig. 3(a) and (b) shows the XRD patterns for **1** (as-prepared) and **1-recry**, respectively. Both are in good agreement with the simulation pattern (Fig. 3(d)) based on the structural data of **1-recry**, and this demonstrates that **1** is isostructural with **1-recry**. However, as **1** contains 0.8 NO_3^- molecule per formula, the occupancy of K should be 96.7% (=5.8/6.0) when we assume a full (100%) occupancy for the Na site. From the elemental analysis of Na and K in **1**, it is likely that the K site accommodates not only K^+ (occupancy: 88.3%) but also extra Na^+ (occupancy: 8.3%). Such forced Na^+ insertion to the K site was achieved by precipitation of **1** in the presence of excess of Na^+ (and NO_3^-). Conversely, the release of Na^+ and K^+ (and NO_3^-) form **1** occurs under low alkaline ion concentrations (via the recrystallization) to yield **1-recry**. Similar behavior has been reported for $Co(OH)_2$-based layer compounds intercalated with NO_3^- and CO_3^{2-} [29], in which the content of NO_3^- increases when prepared in the presence of huge amount of $NaNO_3$. In this case, the negative charge of NO_3^- is compensated by a partial valence change from Co^{II} to Co^{III}.

The X-ray crystallographic analysis of **2-recy** revealed that it is isostructural with **1-recry** except that the six nitrate O atoms has been replaced with Cl, and the N center be vacant (Fig. S1). The

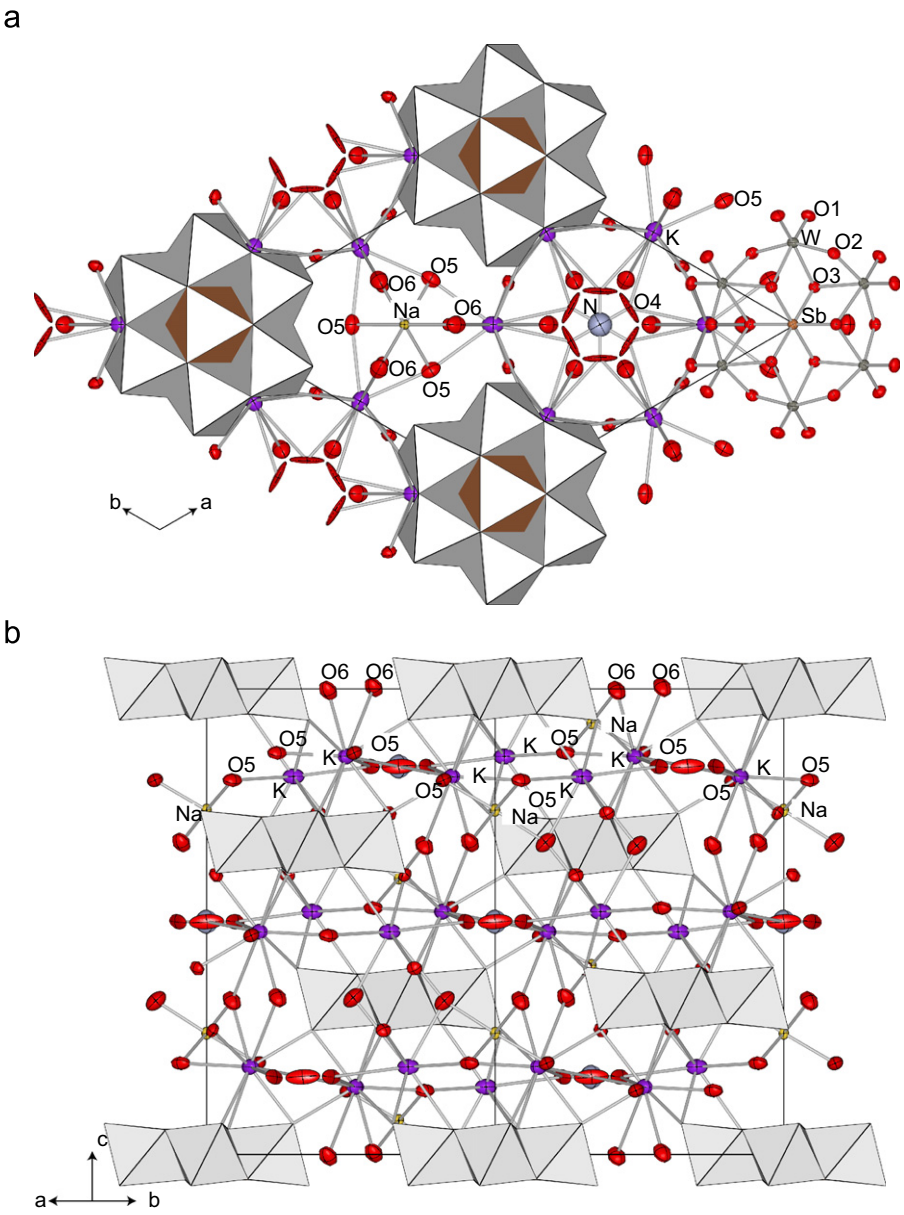

Fig. 1. Crystal structure of **1-recry** viewed parallel to the [0 0 1] (a) and [1 1 0] (b) directions. Thermal ellipsoids are plotted with a probability of 50%.

element analysis showed that the Cl content is only 0.24 per formula unit, corresponding to the population 4% for the each Cl site. Like the compound **1**, **2** is prepared by precipitation with an excess of NaCl, however, Cl content in **2** is only 0.35 per formula unit.

3.2. Dehydration and rehydration behavior

Fig. 4 shows IR spectra of **1** (a), **1-recry** (b), **1-dehyd400** (c), and **1-dehyd500** (d). The spectrum of **1** exhibits intense absorption bands at 890, 930, and ~705 cm^{-1}, which are assignable to ν_{as} based on W=O, W–O–W, and Sb–O bonding in the $[SbW_6O_{24}]^{7-}$ anion, respectively [30]. The peaks at 1355 and 1385 cm^{-1} are due to the absorption by NO_3^-. The spectrum of **1-recry** (Fig. 4(b)) is identical to that of **1** except for lack of the 1385 cm^{-1} band. The peak at 1355 cm^{-1} is attributed to the degenerate stretching mode of the NO_3^- group imposed on the D_{3d} site symmetry [31], which is in accordance with the structural analysis of **1-recry**. The relatively large width of this band is caused by the disordering of both NO_3^- and surrounding K^+. The additional band at 1385 cm^{-1} observed for **1** is attributable to NO_3^- positioned on the site surrounded by both K^+ and extra Na^+ atoms as assumed above. The IR spectrum of **1-dehyd400** (Fig. 4(c)) shows that basic POM structure as well as NO_3^- is retained, although some shift of the POM band and broadening of the NO_3^- band are observed. The thermogravimetry for **1** (Fig. S2) reveals that most of the crystallization water molecules are removed in **1-dehyd400**. The IR bands for the further heated sample **1-dehyd500** are much broadened (Fig. 4(d)), which indicates a decomposition of the POM framework.

The XRD pattern of **1-dehyd400** (Fig. 5(b)) measured at room temperature is successfully indexed based on a trigonal system with lattice constants of $a=11.05$ Å and $c=17.09$ Å, which are smaller than the original axes for **1-recry**. The XRD pattern for the in-situ high-temperature (375 °C) measurement (Fig. 6, cross) is similar to that for **1-dehyd400** except for some shifts of diffraction peaks and line broadening due to thermal effects. In order to

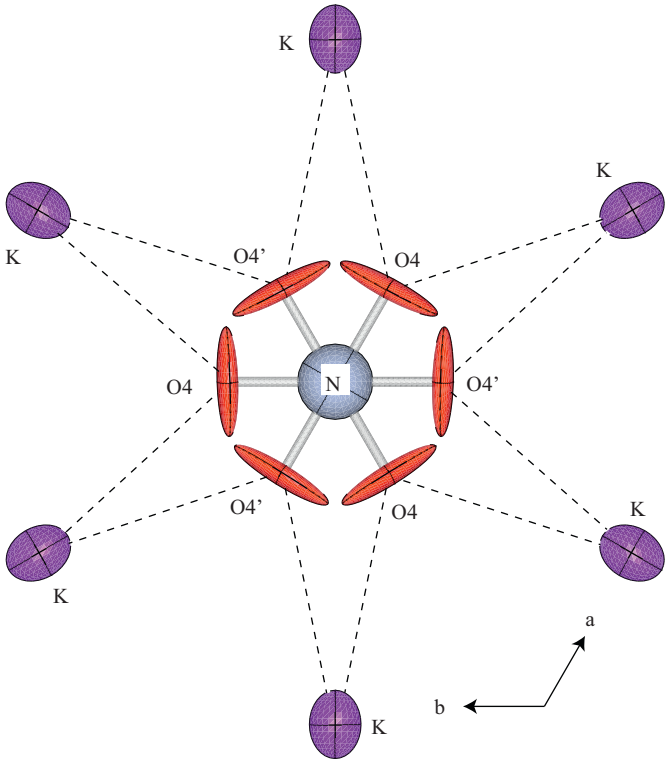

Fig. 2. NO_3^- group and surrounding K^+ cations in **1-recry** viewed parallel to the c axis. The O4' is the $\bar{3}m$ symmetry-related atoms of O4.

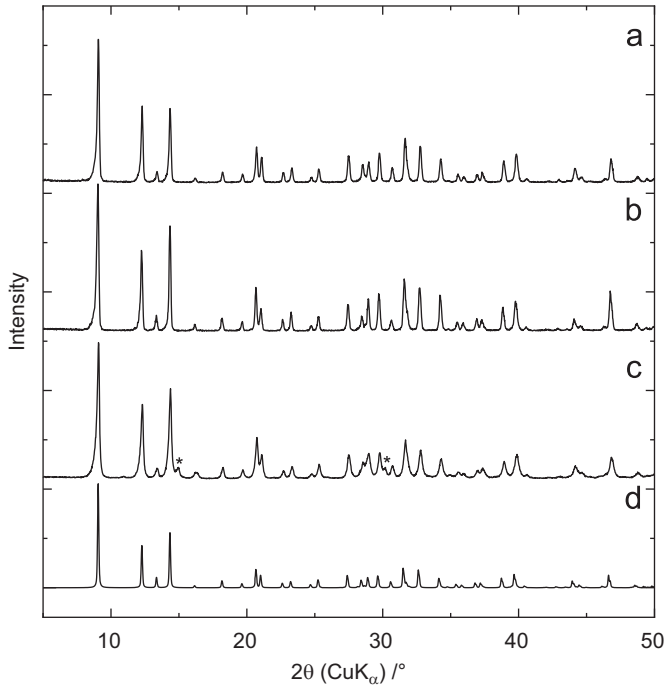

Fig. 3. Observed XRD patterns of **1** (a), **1-recry** (b), re-hydrated sample of **1-dehyd400** (c), and calculated XRD pattern of **1** (d). The asterisked peaks in (c): (Na,K)$SbWO_6$.

estimate the dehydrated structure, diffraction patterns were simulated based on the simple contracted structure model (Fig. 5a right, a=11.05 Å and c=17.09 Å), in which relative positions of $[SbW_6O_{24}]^{7-}$, Na^+, K^+, and NO_3^- in **1-recry** are

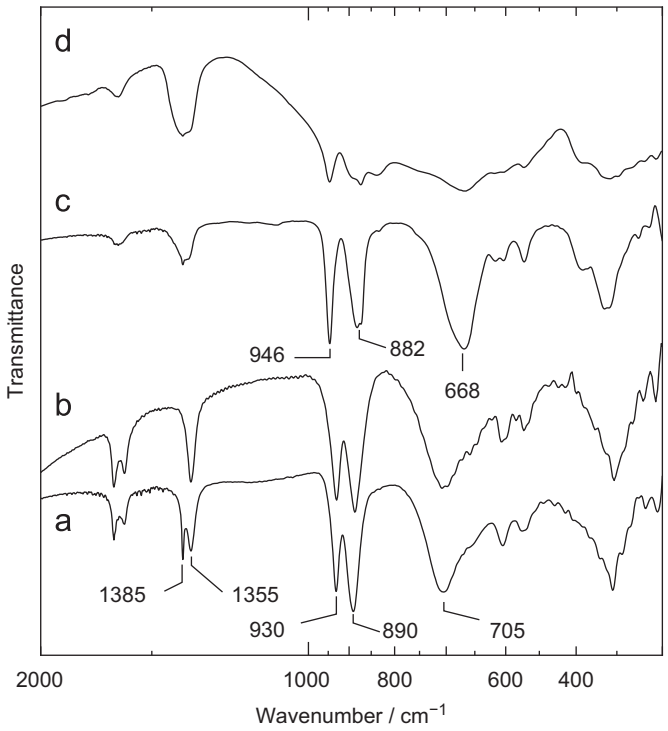

Fig. 4. IR spectra of **1** (a), **1-recry** (b), **1-dehyd400** (c), and **1-dehyd500** (d).

retained. Fig. 5(a) displays the simulated pattern, which exhibits a remarkable disagreement with the observed pattern (Fig. 5(b)); the relative intensities of 021, 202, and 122 are much lower and that of 030 is larger than the observed peaks. In this structure model, one may observe a short intermolecular O···O contact with a distance of ca. 2.37 Å (broken lines in Fig. 5(a) right top). The effective number of this contact is six per anion, and resulting repulsion energy would destabilize the structure. Then we attempted to rotate the $[SbW_6O_{24}]^{7-}$ anion by 30° around the $\bar{3}$ axis, because the operation effectively avoid these O···O contacts. Note that this rotation extinguishes the crystallographic mirror plane (m) of the original space group $R\bar{3}m$, and results in the new space group $R\bar{3}$. Utilizing this 30°-rotated structure as the initial model, we carried out the Rietveld refinement of the XRD pattern at 375 °C. Fig. 6 represents the refinement result. The good agreement between the observed and simulated patterns demonstrates the rotation model to be effective. The refined rotation angle of the anion is 24.85° (based on the W position). The parameters of $[SbW_6O_{24}]^{7-}$ and Na^+ and K^+ cations were successfully refined, however, the position of NO_3^- could not be determined due to the poor quality of the XRD pattern. The Na^+ and K^+ cations are disorderly located at the interstitial positions of the {SbW_6O_{24}}-sheets. The contraction rate along the a-axis (17%) is larger than that along the c-axis (8%). This anisotropic lattice shrinkage is understandable when we consider the initial positions of the water oxygens O5 and O6 in **1-recry**; the removal of O6 located between anions in the {SbW_6O_{24}}-sheet effectively shortens the a-axis (Fig. 1(b)), whereas the removal of O5 located between the sheets causes less influence on the c-axis, because the interlayer spacing is mainly supported by pillaring of O1–K–O3 linkages (Fig. 1). The dehydrated sample of **1** is highly hydroscopic—it absorbs water rapidly on exposure to humid air to recover the original structure (Fig. 3(b)). Formation of (Na,K)$SbWO_6$ in trace amounts observed for the 400 °C-treated samples (Figs. 3(c) and 5(b) asterisked) is probably caused by thermal decomposition. Again, we point out the similarity to

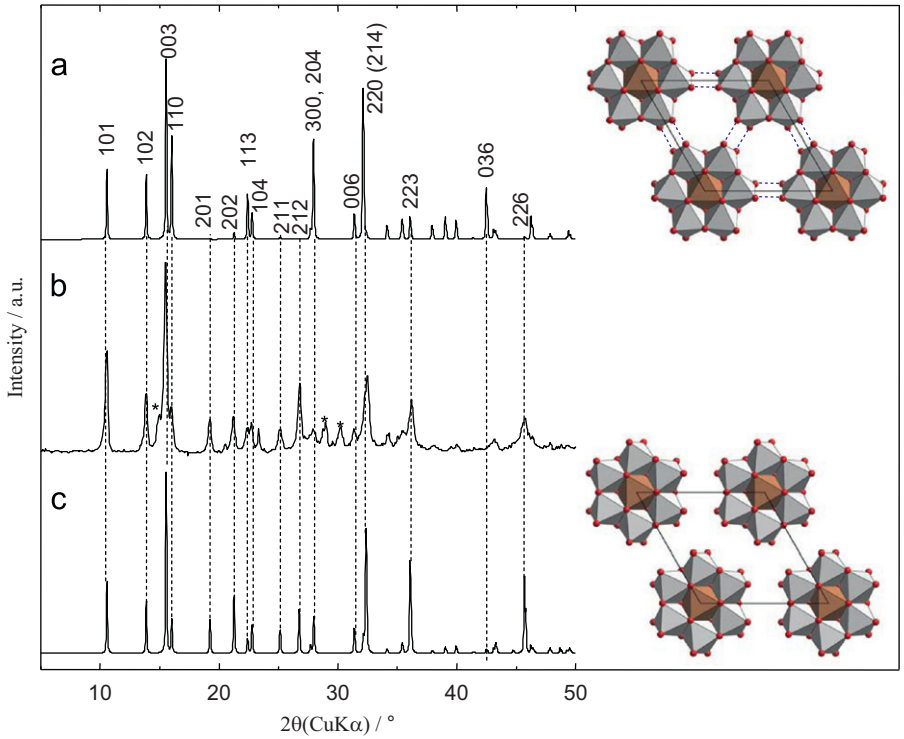

Fig. 5. Observed (b) and simulated (a, c) XRD patterns of **1-dehyd400**. (a) Calculated pattern (left) and the contraction model (right) used for the simulation. The short intermolecular O · · · O contacts are drawn with broken lines in right top (see text). (b) Observed pattern measured at room temperature. (c) Calculated pattern (left) and the 30°-rotated model (right bottom) used for the simulation. For clarity, the Na^+ and K^+ cations and water oxygen atoms are omitted in the models.

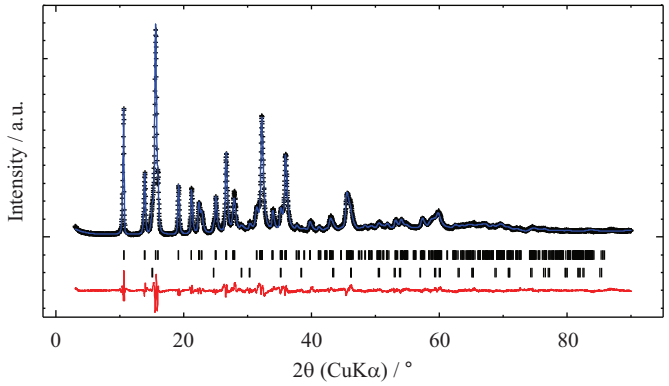

Fig. 6. Results for the Rietveld refinement of the XRD pattern of **1** measured at 375 °C. +: I_{obs}, —:I_{calc}, |: diffraction angles for the sample phase (upper) and $KSbWO_6$ impurity (lower), bottom curve: $I_{obs}-I_{calc}$.

LDHs, which are known to show a reversible thermal dehydration and re-hydration property [32].

The dehydration and rehydration behavior of **2** bears a resemblance to that of **1**. An exception is that the total dehydration is achieved at 500 °C (**2-dehyd500**) as shown in the XRD analysis (Fig. S3) and IR spectroscopy (Fig. S4). Heat treatment at 400 °C (**2-dehyd400**) yields a mixture of **2** and **2-dehyd500**. Since the XRD pattern of **2-dehyd500** is similar to that of **1-dehyd400**, both has the same structure, i.e. the anion rotated structure is effective in **2-dehyd500**.

3.3. Ionic conduction of the dehydrated samples

Impedance spectra for **1-dehyd400** are represented in Fig. 7. The Z_{real} vs. Z_{img} plots at 200–400 °C do not show simple semicircles, but monotonically increasing curves with a decrease

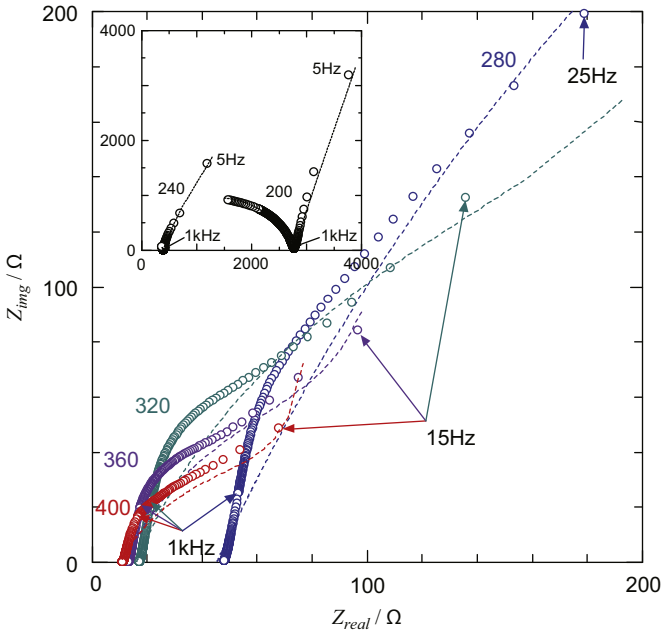

Fig. 7. Impedance spectra of **1-dehyd400** measured at 200–400 °C. Open circles: observed. Broken curves: fitted spectra based on the equivalent circuits shown in Scheme 3. The inset values denote the measurement temperatures.

of frequency. The intercepts on the Z_{real} axis reveal a presence of low resistant component in this system. Taking into account that the measurement was carried out for the mechanically compressed powders clipped with the Pt plates, resistivities at grain boundary and sample/Pt plate interface would be higher than that of the bulk. Therefore, the observed low resistivities are attributed to the bulk property. Scheme 3(a) displays a predicted equivalent

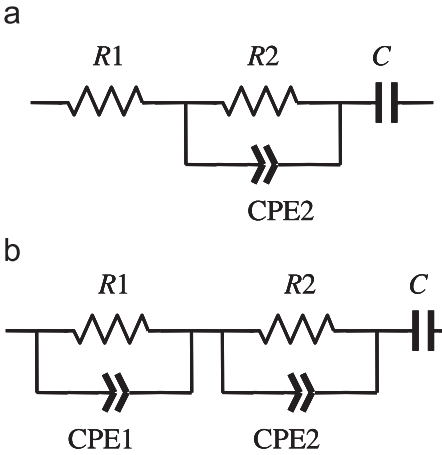

Scheme 3. Equivalent circuits for **1-dehyd400** in the temperature ranges 300–400 °C (a) and 200–280 °C (b).

circuit valid in the 300–400 °C range (Fig. 7). The parameters $R1$ and $R2$ correspond to the resistances of the bulk and grain boundary, respectively. Note that a constant phase element (CPE2) parallel to $R2$ is crucial to fit the observed data. The fitted curves (dotted line in Fig. 7), however, still have deviation from the observed plots. Grain–grain contacts in the mechanically compressed sample should be highly inhomogeneous, and it would be difficult to simulate the spectra successfully using the simple equivalent circuit shown in Scheme 3(a) and (b). At lower temperatures, 200–240 °C, the bulk property gained an observable capacitance (Fig. 7 inset), which was describable with another CPE (CPE2) in the equivalent circuit (Scheme 3(b)). The optimized parameters for the impedance analysis were listed in Table S5.

To confirm the ionic conduction in **1-dehyd400**, we measured the dc conductivity at 400 °C as a function of time (0–100 min) after an application of dc voltage (1.0 V). The sample disk is sandwiched by the Pt plates as blocking electrodes. The result is shown in Fig. S7, in which dc conductivity (closed circle) decreased rapidly with time compared with the ac conductivity (open circle), approaching a steady value. The final dc conductivity is ~3 orders of magnitudes lower than the ac conductivity. We conclude that the conduction is purely ionic with an estimated ionic transference number ~0.999. The conducting ion in **1-dehyd400** was determined by dc potentiostatic electrolysis (2.0 V 24 h) of the sample disk (1.5 mm thick) at 400 °C in air using the Pt plate electrodes. Fig. 8(a) shows the XRD pattern of products on the cathode-side surface, and Fig. 8(b) displays distribution profiles of K, Sb, and W analyzed by EDX as a function of depth from the cathode side surface. It should be noted that the profiles in Fig. 8(b) are somewhat ill-defined because the probe size (ca. 0.12 mm) of the EDX analysis is comparable to or larger than the thicknesses of product layers. Profile for Na was unobservable due to a low EDX sensitivity. At least two layers (inner and outer) were found on the cathode side; K was condensed mainly in the inner layer, Sb was condensed in the outer layer, and W was absent in the outer layer. The XRD pattern consists of diffractions of $NaSbO_3$ [33,34], $(Na,K)SbWO_6$ [35,36], and unidentified phase(s). These results suggest that the outer and inner layers are $NaSbO_3$ and $(K,Na)SbWO_6$, respectively. Therefore, it is concluded that conductive ions in the dehydrated **1** are Na^+ and K^+. A presumable reactions on the cathode side are as follows; initial reduction products, metallic Na and K, immediately bind to aerobic oxygen to form Na_2O and K_2O, followed by reaction with $[SbW_6O_{24}]^{7-}$ to yield $NaSbO_3$ and $(Na,K)SbWO_6$. The high Sb contents at the two layers are caused by the last two products.

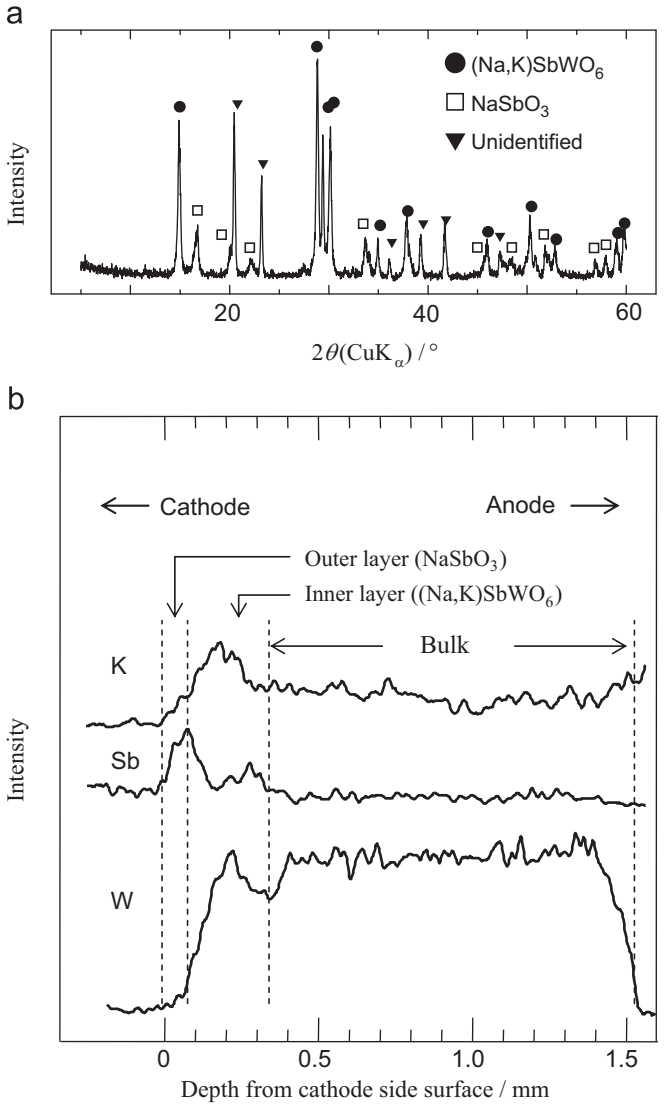

Fig. 8. (a) XRD pattern of cathode side surface of the **1-dehyd400** disk after dc-electrolysis. (b) Distribution profiles for K, Sb, and W analyzed by EDX as a function of depth from the cathode side surface.

Temperature dependence of conductivities (σ) for **1-dehyd400**, **1-recry-dehyd400**, and **2-dehyd500** are represented in Fig. 9. The successful impedance analysis for **1-dehyd400** using the equivalent circuits (Scheme 3) allowed to resolve the conductivities into the bulk and grain boundary components (Table S5). At 400 °C, the bulk conductivity for **1-dehyd400** is the highest of all the samples; it marks $\sigma = 1.2 \times 10^{-2}\ \Omega^{-1}\ cm^{-1}$. This σ level is smaller than that for Na^+ β-alumina single crystals [37] by a factor of two. The grain boundary σ, which is 1–1.5 orders of magnitude lower than the bulk, is relatively high when we take it into account that the sample specimen is the compressed powder in which intergrain contacts would be loose and inhomogeneous. It is also noticeable in Fig. 9 that recrystallization of **1** (**1-recry**), that involved loss of half amount of NO_3^-, caused marked reduction of σ. Furthermore, **2-dehyd500** containing no NO_3^- has much less σ than the dehydrated **1-recry** by a factor of three at 400 °C. These results demonstrate some contributions of NO_3^- to the σ. An apparent role of NO_3^- is that it accompanies extra cations (Na^+ and K^+) for charge compensation, and results in an enhancement of conduction carriers. Although the NO_3^- position is undetermined from the structure refinement, it might affect the cation

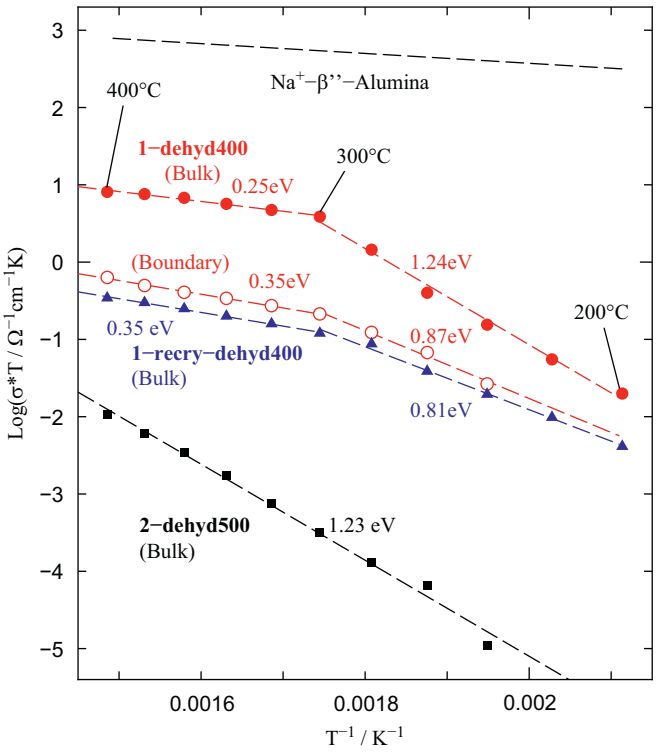

Fig. 9. Temperature dependence of conductivity (σ) for **1-dehyd400**, **1-recry-dehyd400**, and **2-dehyd500**. The values in eV unit are activation energies in the temperature range of 220–400 °C (for **2-dehyd500**) and the separate ranges of 200–300 °C and 300–400 °C (for **1-dehyd400** and **1-recry-dehyd400**). Datum for Na^+-β''-alumina is also plotted for reference.

conduction by electrostatic interaction. Note that similar situation has been suggested for non-stoichiometric Na^+-β''-alumina; insertion of excess of Na^+ and charge compensating O^{2-} into the interlayer space (conduction plane) are responsible for high conduction [38]. As shown in Fig. 9, the plot for **1-dehyd400** (bulk) has a bend point at 300 °C, exhibiting quite different activation energies at higher (0.25 eV) and lower (1.24 eV) temperatures. Since the bend point is less clear for **1-recry-dehyd400** and unobservable for **2-dehyd500**, the NO_3^- group might contribute this transition. The DTA (Fig. S5) and in-situ XRD for **1-dehyd400** (Figs. 5(b) and 6) indicate no signs of endothermal or exothermal peak and major structural change between the room temperature and 400 °C, respectively, suggesting a second-order transition at around 300 °C.

4. Conclusions

In the present study, the structural and functional analogies between the LLA type POMs and the CdI_2(or brucite) type layered metal oxides containing $\{MO_2\}$-sheets were described. We observed inclusions of NO_3^- and Cl^- anions (and charge compensating Na^+ and K^+ cations), and reversible dehydration–rehydration in $Na_2K_5[SbW_6O_{24}]\cdot 12H_2O$ retaining its LLA structure. The former occurred without structural change, while the latter involved the rotation of the $[SbW_6O_{24}]^{7-}$ anion by 24.85° in order to avoid intermolecular O···O contacts along with the shrinkage of lattice. Another significance of this study was the relatively high alkaline ion conductions in dehydrated samples. The highest total conduction was achieved in **1-dehyd400** ($1.2\times10^{-2}\,\Omega^{-1}\,cm^{-1}$ at 400 °C) containing 0.8 NO_3^- per $[SbW_6O_{24}]^{7-}$ anion. A parallelism between the Na_2O insertion into the stoichiometric Na^+-β''-alumina ($Na_2O\cdot 11Al_2O_3$) and the $NaNO_3$ insertion into the parent $Na_2K_5[SbW_6O_{24}]\cdot 12H_2O$ is also pointed out—both give rise to the dramatic increase in bulk conductivity. However, the role of NO_3^- in the conduction plane of was unidentified. It is of interest that the grain boundary contribution in the conductivity was relatively large despite the simple mechanical pressing of the powder sample.

Supplementary data available

Crystallographic information files (CIF) for **1-recry** and **2-recry**. Tables for geometric parameters of **1-recry** and **2-recry** (Tables S1 and S2). Crystal structure plot for **2-recry** (Fig. S1). TG analysis for **1** (Fig. S2). XRD patterns of **2**, **2-dehyd400** and **2-dehyd500** (Fig. S3). IR spectra for **2**, **2-dehyd500** and **2-dehyd600** (Fig. S4). Cycled DTA for **1-dehyd400** (Fig. S5). Details on the Rietveld refinement for the dehydrated sample at 375 °C (Table S3, Table S4, and Fig. S6). The dc conductivity for **1-dehyd400** at 400 °C (Fig. S7). These materials are available free of charge via the Internet.

Appendix A. Supporting information

Supplementary data associated with this article can be found in the online version at doi:10.1016/j.jssc.2011.01.033.

References

[1] J.S. Anderson, Nature (London) 150 (1937) 850.
[2] A. Perloff, Inorg. Chem. 9 (1970) 2228.
[3] H.T. Evans, Acta. Crystallogr. B30 (1974) 2095.
[4] K. Nomiya, T. Takahashi, T. Shirai, M. Miwa, Polyhedron 6 (1987) 213.
[5] M.T. Pope, Heteropoly and Isopoly Oxometalates, Springer-Verlag, Berlin, 1983.
[6] A. Müller, F. Peters, M.T. Pope, D. Gatteschi, Chem. Rev. 98 (1998) 239.
[7] F.S. Galasso, Structure and Properties of Inorganic Compounds, Pergamon Press, Oxford, UK, 1970.
[8] W.I.F. David, J.B. Goodenough, M.M. Thackeray, M.G.S.R. Thomas, Rev. Chim. Miner. 20 (1983) 636.
[9] J. Akimoto, Y. Gotoh, Y. Osawa, J. Solid State Chem. 141 (1998) 298.
[10] V. Rives, M.A. Ulibarri, Coord. Chem. Rev. 181 (1999) 61.
[11] A. Wilson, A.D. Yoffe, Adv. Phys. 18 (1969) 193.
[12] M.S. Whittingham, Chem. Rev. 104 (2004) 4271.
[13] U. Lee, Y. Sasaki, Bull. Korean Chem. Soc. 8 (1987) 1.
[14] O. Nakamura, T. Kodama, I. Ogino, Y. Miyake, Chem. Lett. (1979) 17.
[15] K.D. Kreuer, M. Hampele, K. Dolde, A. Rabenau, Solid State Ionics 28-30 (1988) 589.
[16] A. Dolbecq, C. Peloux, A.-L. Auberty, S.A. Mason, P. Barboux, J. Marrot, E. Cadot, F. Sécheresse, Chem. Eur. J. 8 (2002) 350.
[17] G.M. Sheldrick, SHELX-97, Program for Crystal Structure Solution, University of Gettingen, Germany, 1997.
[18] D.J. Watkin, C.K. Prout, J.R. Carruthers, P.W. Betteridge, CRYSTALS Issue 10, Chemical Crystallography Laboratory, Oxford, UK, 1996.
[19] CrystalStructure 3.8, Crystal Structure Analysis Package, Rigaku and Rigaku/MSC, Tokyo, 2000–2002.
[20] T. Higashi, SHAPE, Program to obtain Crystal Shape using CCD Camera, Rigaku, Tokyo, 1999.
[21] T. Higashi, NUMABS, Numerical Absorption Correction, Rigaku, Tokyo, 1999.
[22] H.M. Rietveld, J. Appl. Crystallogr. 2 (1969) 65.
[23] F. Izumi, T. Ikeda, Mater. Sci. Forum 198 (2000) 321.
[24] A.S. Bondarenko, G.A. Ragoisha, EIS Spectrum Analyser, 2008, 〈http://www.abc.chemistry.bsu.by/vi/analyser/〉 .
[25] H. Naruke, T. Yamase, Acta Crystallogr. C48 (1992) 597.
[26] J.K. Nimmo, B.W. Lucas, Acta Crystallogr. B32 (1976) 1968.
[27] J.K. Nimmo, B.W. Lucas, J. Phys. C 6 (1973) 201.
[28] H.M. Lu, J.R. Hardy, Phys. Rev. Ser. 3 (B44) (1991) 7215.
[29] R. Xu, H.C. Zeng, Chem. Mater. 15 (2003) 2040.
[30] M.H. Alizadeh, A.R. Salimi, Spectrochim. Acta A65 (2006) 1104.
[31] M.H. Brooker, D.E. Irish, Can. J. Chem. 48 (1969) 1183.
[32] S.K. Yun, T. Pinnavaia, J. Chem. Mater. 7 (1995) 348.
[33] N. Schrewelius, Z. Anorg. Allg. Chem. 238 (1938) 241.
[34] B. Wang, S.C. Chen, M. Greenblatt, J. Solid State Chem. 108 (1994) 184.
[35] C. Michel, D. Groult, B. Raveau, Mater. Res. Bull. 8 (1973) 201.
[36] C. Michel, D. Groult, A. Deschanvres, B. Raveau, J. Inorg. Nucl. Chem. 37 (1975) 251.
[37] J.L. Briant, G.C. Farrington, J. Solid State Chem. 33 (1980) 385.
[38] K. Edström, J.O. Thomas, Acta. Crystallogr. B47 (1991) 635.